ACTA IMEKO
ISSN: 2221-870X
December 2024, Volume 13, Number 4, 1 - 9

Low-cost UV-induced fluorescence sensor for monitoring aromatic hydrocarbons in coastal marine water

Fabio Lo Savio[1], Giovanni Maria Grasso[2], Giuseppe Maccarrone[3]

[1] *DICAr, University of Catania, V. S. Sofia, 54, 95123 Catania, Italy*
[2] *DIEEI, University of Catania, V.le A. Doria, 6, 95123 Catania, Italy*
[3] *DSC, University of Catania, V.le A. Doria, 6, 95123 Catania, Italy*

ABSTRACT
Nowadays the coastal waters of the Mediterranean Sea are increasingly affected by pollution from aromatic hydrocarbons. Therefore, in order to implement damage minimization actions, a continuous monitoring system with rapid response is needed. The most effective local method for distinguishing aromatic hydrocarbons from salt water is UV-induced fluorescence. This paper describes the design and building of a UV-induced fluorescence sensor that, mounted on board a sensor-buoy, detects the presence or absence of the pollutant in any atmospheric condition. The sensor consists of a measuring chamber, in which the water, loaded by a submersible pump, maintains a constant level thanks to a small siphon. The detection system, consisting of a UVC-LED and a phototransistor that responds in the visible light band, is located in the upper part of the chamber. *In vitro* tests, performed by comparing the sensor results with those obtained from a spectrofluorometer, have shown good sensitivity, repeatability, and accuracy, despite the inexpensiveness and low energy consumption of the sensor. An important goal achieved by the design and building methodology is that the sensor is able to withstand harsh weather conditions, the corrosive action of salt water and biofouling.

Section: RESEARCH PAPER

Keywords: UV-induced fluorescence; aromatic hydrocarbons; measurement; sensor buoy; seawater monitoring

Citation: F. Lo Savio, G. M. Grasso, G. Maccarrone, Low-cost UV-induced fluorescence sensor for monitoring aromatic hydrocarbons in coastal marine water, Acta IMEKO, vol. 13 (2024) no. 4, pp. 1-9. DOI: 10.21014/actaimeko.v13i4.1749

Section Editor: Andrea Scorza, Università degli Studi Roma Tre, Italy

Received January 16, 2024; **In final form** May 9, 2024; **Published** December 2024

Corresponding author: Fabio Lo Savio, e-mail: fabio.losavio@unict.it

1. INTRODUCTION

A serious problem linked to human action, which mainly affects coastal waters [1], [2], is the accidental or intentional spillage of aromatic hydrocarbons into the sea [3]. While accidental spills of oil from coastal oil platforms, storage tanks, and subsea pipelines or discharges into the sea from rivers [4] and for long-range weathering [5], [6] can occur, on the other hand, despite being prohibited by stringent regulations, washing ship bilges into the sea produces the release of large quantities of oily residues. These are the main sources in oil pollution of coastal waters, especially in confined marine environments such as the Mediterranean Sea [7]-[9]. In addition to being very persistent and poorly soluble in water, hydrocarbons are fat-soluble. In this way they can easily penetrate cell membranes to deposit in the fatty tissues of various aquatic organisms, thus entering the food chain [6].

Under natural conditions, all aromatic hydrocarbons occur in the solid state and many of them are naturally contained in coal, crude oil, and the products deriving from its refining (gasoline, diesel fuel, and lubricating oils) [10]. In the sea, if not produced directly by spills from submarine pipelines, the aromatic hydrocarbons initially tend to concentrate in the surface layer of water [11], and then bind to marine sediments and with them settle on the bottom [12]. The great ability to penetrate the food chain makes aromatic hydrocarbons particularly harmful to humans, as they are classified as carcinogenic, mutagenic, and teratogenic [13], [14]. Therefore, continuous monitoring becomes essential, with particular reference to surface waters. The most suitable technologies for this monitoring can be applied on a large scale by aerial or satellite remote sensing. One technique consists in comparing the apparent temperature of hydrocarbons and water with infrared imaging cameras [15], and another is based on the evaluation of the influence of floating oil slicks on the Bragg waves, typically generated by seawater, using the SAR-Radar (Synthetic Aperture Radar) [16], still, another uses LiDAR (Laser Imaging Detection and Ranging) which, by

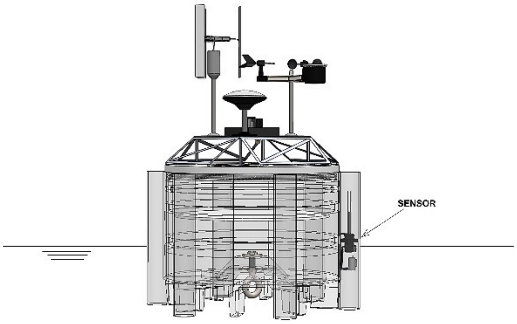

Figure 1. 3D CAD drawing of the buoy body and sensor location.

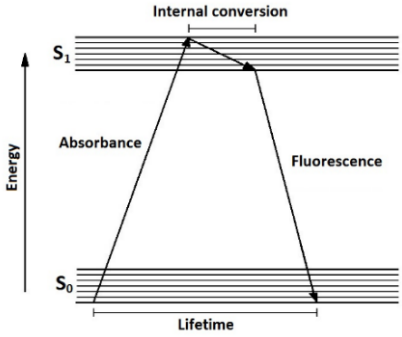

Figure 2. Energy diagram of fluorescence according to Jablonski.

emitting monochromatic light by means of a laser, and collecting the light reflected by the pollutants on the surface by means of a telescope/photomultiplier system, is able to distinguish the elements analysed from the water of the sea [17]-[19].

Local monitoring is also possible, to be performed *in situ* or *in vitro*, through the laboratory analysis of samples collected at sea [20]. Among the most widespread techniques for local monitoring are the Gas Chromatography associated with Mass Spectrometry (GC/MS) [21], High-performance Liquid Chromatography (HPLC) [22], Semi-Permeable Membrane Devices (SPMDs) [23], the Surface-Enhanced Raman Scattering (SERS) [24], [25] and UV Fluorescence spectrometry [11], [26], [27].

The oldest technique for identifying PAHs (Polycyclic Aromatic Hydrocarbons) in seawater is the GC/MS. However, due to the low concentration levels to be quantified in water samples, an enrichment step is required before chromatographic analysis [21]. HPLC is a more advanced method of chromatography, in fact it allows the separation of PAHs dissolved in a sample of saltwater through a solvent that a pump drives towards a separation column which, subsequently, sends the various constituents to a detector to carry out a qualitative and quantitative analysis [28]. SPMDs consist of a thin layer of a neutral lipid (triolein) placed inside a thin-walled low-density polyethylene tube. SPMDs allow the bioavailability and bioconcentration potential of organic contaminants to be measured [29]. SERS enhances Raman scattering of molecules supported by certain nanostructured materials. It enables structural fingerprinting of PAHs through plasmon-mediated amplification of electric fields or chemical enhancement. All these methodologies involve sampling at sea, followed by *in vitro* analyses performed in the laboratory.

UV fluorescence spectrometry is one of the few techniques that allows both *in situ* measurement of pollutants on the water surface and *in vitro* analysis of samples collected at sea. This is obtained by comparing UV fluorescence, induced by polarized light, of floating hydrocarbons with respect to seawater [11]. Their highly fluorescent nature has made molecular fluorescence spectrometry a very popular technique for hydrocarbon analysis. Furthermore, the tested samples are not damaged in the process and no dangerous by-products are generated. Another important advantage of the technique applied to hydrocarbons floating on the surface is given by the proportionality of the concentration of aromatic hydrocarbons with their fluorescence intensity in diluted conditions (i.e. when the optical density is less than 1 %) [30].

Fluorescence excitation of aromatic hydrocarbons is generally achieved through a coherent light beam from a UV-laser xenon lamp, while the consequent detection of induced fluorescence is carried out with spectrofluorometers [31], [32].

The sensor for the detection of aromatic hydrocarbons described in this paper is part of the project for the construction of a sensor-buoy for the monitoring of the Ionian coastal waters, and thus falls within the scope of the local observation [33]. The buoy is cylindrical in shape (φ = 600 mm) and has six external tubes (φ = 80 mm) circumferentially arranged at 60° from each other (Figure 1). Each of the tubes, open at the bottom to allow water to enter, houses a sensor for monitoring the fundamental parameters of the surface water (salinity, turbidity, pH, temperature, presence of hydrocarbons, and dissolved oxygen). The buoy is equipped with numerous other sensors, located inside it and on the upper part, which monitor the local weather conditions (pressure, air temperature outside and inside the buoy, humidity, wind speed and direction, etc.) as well as the dynamic conditions of the water through the relative movements of the buoy (height, speed, and direction of the wave).

The fact that the buoy must be released for long periods at sea creates the need to build sensors that are low-cost, resistant, and require a low power supply. To meet all these needs, in the hydrocarbon-monitoring sensor described in this study, a UV-light LED as the source of fluorescence excitation has replaced the UV laser [34], [35], while the spectrometry of the emitted fluorescence is guaranteed by a phototransistor suitably shielded by a bandpass filter. Therefore, the sensor consists of commercially available low-cost devices: a far UVC-LED (Silanna - SF1-3T9B5L1) with a peak wavelength of 235 nm and an ambient light sensor (Vishay SC - TEMT6200FX01) shielded by a visible bandpass filter (Pixelteq - FWHM 485 nm) were used respectively as the light source and the optical detector.

2. MATERIALS AND METHODS

2.1. Aromatic hydrocarbons fluorescence

As mentioned in Section 1, aromatic hydrocarbons exhibit a strongly fluorescent behaviour when excited by UV rays. This is evident from the simple observation of the water surface inside ports, where gasoline or diesel residues are distinguished by the emission of light in the visible spectral band when illuminated by the ultraviolet light of the sun.

As known, fluorescence occurs when, due to the absorption of UV rays, the hydrocarbon electrons acquire such an energy as to reach an excited state S_1. They, subsequently, return to the ground electronic state (S_0) compensating for the sudden loss of energy by emitting a photon of fluorescent light. The whole cycle lasts a few nanoseconds [36]. The Jablonski diagram, illustrating the phenomenon described above, is shown in Figure 2.

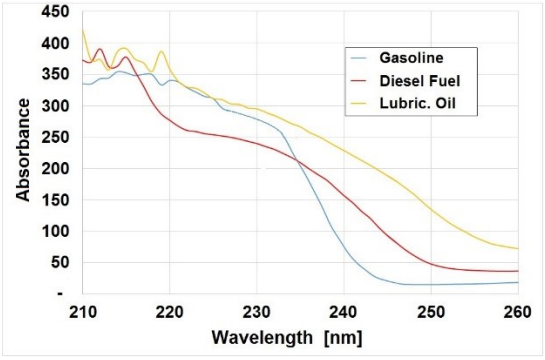

Figure 3. Absorbance spectra of the tested hydrocarbons.

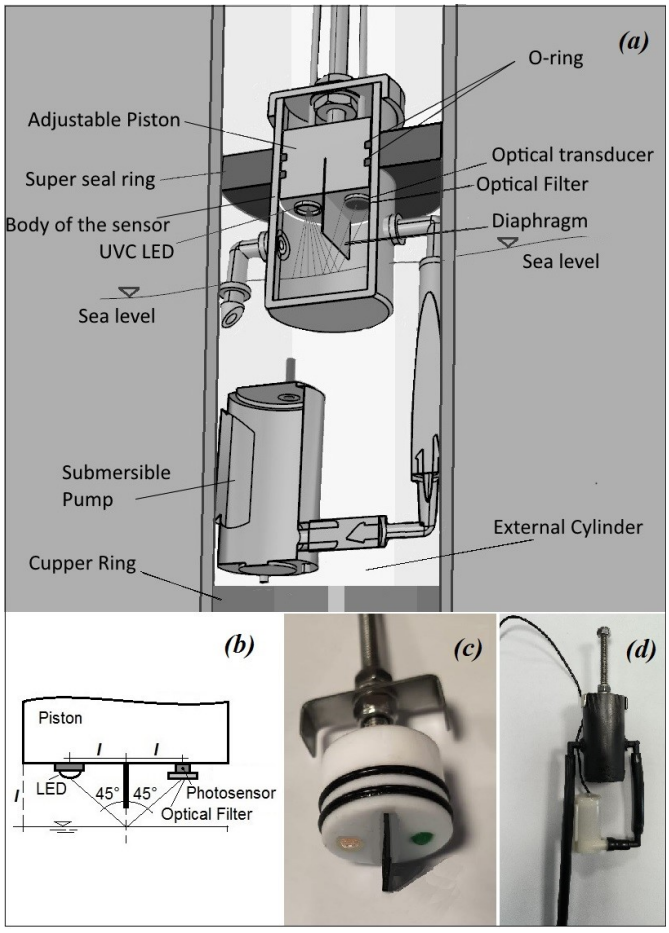

Figure 4. (*a*) 3D CAD drawing of the sensor inside its housing tube; (*b*) drawing for calculating the distance between the free surface and the photosensor (*c*) a particular of the sensor: PTFE piston with LED/detector system; (*d*) the assembled device.

2.2. Excitation sources of fluorescence

Fluorescence induced by UV light is the most versatile technique for analysing hydrocarbons in marine water as, unlike radar, IR or visible remote sensing systems, it is able to detect even a thin film of oil on the surface [11]. Thanks to the short acquisition times, which increase its responsiveness, it is a popular technique for continuous monitoring and can be used effectively both day and night, since it employs sensors that are less affected by the illuminance conditions [37].

Once the UV photon has been absorbed, the molecule of the tested compound emits a fluorescence spectrum, providing a sort of characteristic fingerprint of each fluorescent component present in the pollutant. Therefore, it will be possible to detect both organic and inorganic materials, provided they have fluorescence capabilities.

As a UV-light source to be used in the sensor covered by the paper, the authors selected LED diodes. There can be monochromatic or white light LEDs [37]-[39]. The former are available in a wide range of wavelengths and can also be used in matrices of different colours [34], the latter require monochromator filters of different colours to pass only the desired wavelengths. Since they require a low supply voltage and are small-sized, LEDs are the most used for portable instruments. Finally, they do not emit in the infrared, as happens in xenon lamps, making the use of thermal filters unnecessary.

To choose the UV-LED with an emission wavelength suitable for exciting the most widespread aromatic compounds in Mediterranean coastal waters, the absorbance spectra of these compounds were measured in the laboratory. The plots, obtained using a Jasko V-530 spectrophotometer, are summarized in Figure 3.

As can be seen from the plots in Figure 3, relating to gasoline, diesel fuel, and lubricating oil, the maximum excitation response occurs in the range between 210 and 240 nm. This is because the main aromatic components of the tested compounds are monocyclic, i.e. with only one benzene ring, excited by wavelengths belonging to the far UVC range. For this reason, the authors selected an LED source that emits UV light at 235 nm.

3. UV-INDUCED FLUORESCENCE SENSOR

As stated in Section 1, the UV-induced fluorescence sensor will belong to a set of transducers that, operating in coastal waters on a small buoy, will be subjected to thermal gradients, wind, precipitation, and continuous salt-water action, as well as the attack by encrusting organisms (biofouling). For this reason, it is necessary for the sensor to be resistant and inexpensive, but at the same time maintain a good level of accuracy.

3.1. Design and implementation of the sensor

Figure 4*a* shows the 3D CAD drawing of the realised sensor. The body of the sensor consists of a hollow carbon cylinder (φ = 30 mm) closed at the bottom, forming a chamber since, as already stated, the reading of the fluorescence produced by the hydrocarbon layer floating on the water surface must be performed in air and the liquid level must remain constant, at a well-defined distance from the source/detector system, and unperturbed. For this reason, this system will be placed above the chamber where the water will enter through a small siphon.

A submersible pump will load the water at regular intervals dictated by a microcontroller placed in the body of the buoy. The water level inside the chamber was calculated so that the angle between the incident beam (UVC) and the emerging one (fluorescence) is 90°. This angle causes the component of the beam incident on the photodetector to be zero (cos(90°) = 0) (Figure 4*b*).

The LED/photodetector system separated by a vertical carbon septum, which prevents reverberation of the direct LED light on the detector, was mounted on the PTFE (Teflon) piston shown in Figure 4*c*. The piston is hollow inside to allow the housing of this optical system and with a double seal (O-rings) to isolate the upper part from the water, and can slide inside the carbon cylinder.

Of course, in this operating typology, the septum is superfluous, as the photodetector is insensitive to UVC light, but

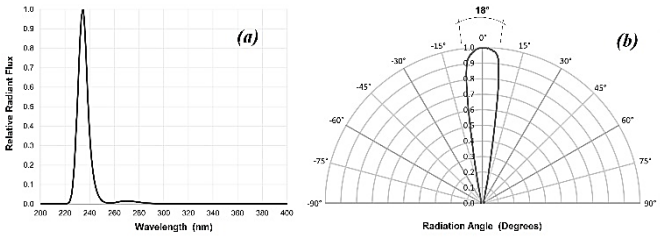

Figure 5. (a) Relative spectral sensitivity and (*b*) Radiation pattern of the SF1-3T9B5L1 Silanna UV-LED.

if you want to use a white light LED or a matrix of LEDs with different wavelengths, it will assume fundamental importance.

The distance between the free surface of the liquid and the source/detector system in the measurement chamber (*l* in Figure 4*b*) must be constant and greater than the height of the vertical septum, in order to allow the UV light to excite the fluorescence of the hydrocarbons below the photosensor. To achieve this objective, the internal piston is equipped with a bracket guided by a threaded screw (both in AISI-316 steel) (Figure 4*c*), the adjustment of which allows the required distance to be obtained. The water inlet and outlet were made in AM and glued to the rest of the structure with epoxy resin. The same technology was used to mould both the buoy body and the external cylindrical sensor-holders. The assembled sensor is shown in Figure 4*d*.

The LED used as the emission source is SF1-3T9B5L1 from the Silanna UV Company. It emits in the far UVC range with a peak wavelength of 235 nm (Figure 5a), making it effective even for the detection of monocyclic compounds such as benzene [35]. Having a collimation width of 18° the LED provides a higher irradiance (2.15 mW/sr), which is useful in surveying applications (Figure 5*b*). The supply voltage is 5.8 V.

The phototransistor used to detect the fluorescence emitted in the visible spectrum is the TEMT6200FX01 from Vishay Semiconductors. The relative spectral sensitivity and the radiation pattern of this phototransistor are shown in Figure 6*a* and *b*, respectively.

To build the sensor body, mould and related punch were made in Additive Manufacturing (AM). The moulding process was performed in the Flashforge Photo 13.3" 3D printer. Since the best physical and mechanical properties were obtained with a degree of polymerization greater than 95 %, a post-processing step was required. This 120-minute process was performed inside the printer itself, where both an additional amount of UV light and temperature (100 °C) were provided to achieve the required level of cure.

The volume between mould and the punch was used to place the carbon fibers and subsequently carry out the resin infusion with the Resin Transfer Moulding (RTM) technology.

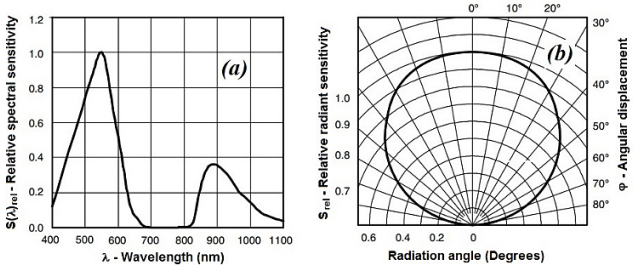

Figure 6. (*a*) Relative spectral sensitivity and (*b*) Radiation pattern of the TEMT6200FX01 from Vishay Semiconductors Phototransistor.

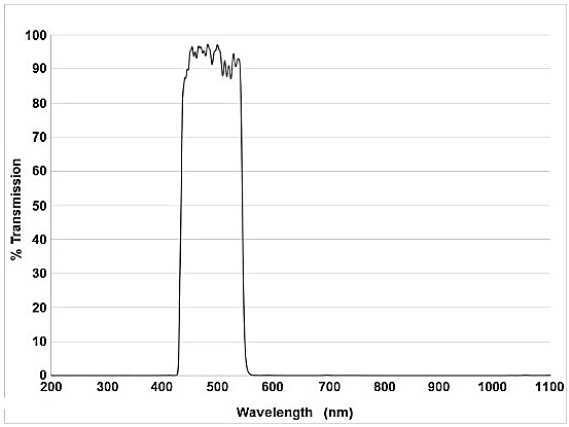

Figure 7. Bandpass filter spectrum.

At the end of the infusion, the thermal post-curing was performed in a special oven for the complete polymerization of the epoxy resin for 6 hours at 110 °C.

3.2. Filtering of the fluorescence signal

Assuming the simultaneous presence of biological substances dissolved in seawater, for an excitation wavelength of 235 nm, the mass of coloured dissolved organic matter (CDOM) will have a fluorescence response around 420 nm (violet region) [40]-[42], while the chlorophyll-*a*, present in the phytoplankton, will respond around 685 nm (red region) [42]. Since most aromatic hydrocarbons react with a fluorescence that varies between 480 nm and 550 nm (blue/green region) [43], the use of a band-pass filter, centered on the wavelength of 485 nm (Pixelteq - FWHM), will allow only the fluorescence related to hydrocarbons to be detected. The spectrum of the bandpass filter used is shown in Figure 7.

3.3. Electronics and emitted signal management

The sensor electronics were located in the central body of the buoy. The wiring diagram is shown in Figure 8. The microprocessor used is the Raspberry PI 4. It manages the sensor (LED, photodetector, and submersible pump) and all the other sensors listed above, supplying power and collecting the measurement data in the times set by the internal clock. The programming was done using the Raspberry Pi OS software. The analog signal supplied by the photodetector was amplified and converted into digital by means of a 16-bit converter (Gravity I2C ADS1115) and then sent to the microprocessor that can memorize it or send it to the PC for immediate reading. Based on its flow rate, the pump was set to operate every 15 minutes for a duration of 11.8 seconds, thus guaranteeing three volumes of chamber washing before carrying out the measurement.

The main geometric, structural, and electrical parameters of the elements constituting the sensor are summarized in Table 1.

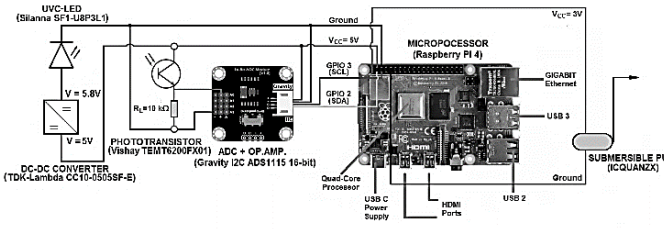

Figure 8. Sensor wiring diagram.

Table 1. The main parameters of the sensor.

Parameters	Elements	Values
Size in mm		162 × 52 × 30
Case material	Sensor	Carbon fibre
	Pump	PVC
	Hoses	Rubber
Power supply voltage in V_{DC}	UV-LED	5.8
	Photodetector	5
	Pump	3
	ADC + Op. Amp.	5
	DC/DC Converter	5
	Raspberry PI	5
Power consumption in W	UV-LED	0.29
	Photodetector	0.1
	Pump	0.3
	ADC + Op. Amp.	0.01
	DC/DC Converter	1.5
	Raspberry PI	0.4
	Total	2.6
Excitation wavelength in nm	UV-LED	235
Emission wavelength in nm	Photodetector	485

3.4. Biofouling and sensor protection

Biofouling represents an unwanted accumulation of microorganisms, plants, algae, and mollusks (barnacles and bivalves) on structures submerged in seawater. Deposition begins with the adhesion of biofilms produced by bacteria (microfouling), followed by larger organisms (macrofouling). This phenomenon is the main factor limiting the use of submerged sensors for oceanographic studies [44]. It was demonstrated that copper, through the oxidized molecules released in water due to erosion, interferes with enzymes on cell membranes and prevents cell division of such organisms [45]. For this reason, a replaceable and expendable copper ring, 10 mm high and 1 mm thick, was fixed inside the lower edge of each of the six tubes hosting the sensors.

4. IN VITRO SENSOR CALIBRATION

To validate the correct functioning of the sensor, the fluorescence of some of the most common polluting elements in coastal waters was tested in the laboratory: gasoline, diesel fuel and lubricating oil. Of course, these are elements composed of various aromatic hydrocarbons, each having its own fluorescence spectrum. The overall emission is, therefore, characterized by a set of characteristic peaks of the wavelengths of the individual oleic components.

4.1. Test with optical spectrofluorometer

As already described in Section 2.2, using a UV/Visible spectrophotometer (Jasko V-530), the absorbance spectra of three of the most widespread polluting hydrocarbons present in the coastal waters of the Mediterranean Sea (gasoline, naval diesel, and lubricating oil), taken at pure state, they were obtained.

After selecting the wavelength of UV light that ensures good fluorescence emission for all tested hydrocarbons (λ_{ex} = 235 nm), the fluorescence spectra of the three compounds were measured using a spectrofluorometer (Varian Cary Eclipse). The excitation wavelength was selected through the right compromise between a range in which the absorbance of the tested compounds was uniform and conspicuous (see Figure 3) and the difficulty in commercially finding UV-LED of a shorter wavelength of 235 nm, to be used in the construction of the sensor.

To obtain the fluorescence spectra, four series of elements were tested, each consisting of five withdrawals from the same sample. The first series contained clean seawater, taken from a protected coastal marine area, in each of the other three enough of a single pollutant was added to the water to obtain a surface layer 1 mm thick. The individual samples were contained in quartz cuvettes with a square section of 10 mm on each side.

The percentage of pollutant added into each cuvette (3.47 %) was chosen to equal that calculated from the ratio between the volume of the layer and that of the seawater inside the measurement chamber of the sensor designed in this study. To obtain the expected thickness (s = 1 mm), a volume of 0.1 ml of pollutant was added to each cuvette for a volume of water of 2.88 ml, corresponding to a height of 28.8 mm.

An example of the frequency response of each series for λ_{ex} = 235 nm is shown in Figure 9*a*. As seen in the emerging spectrum of the detail in Figure 9*b*, the wavelength λ_{em} = 485 nm presents a peak for each of the three pollutants.

Table 2 reports the average values of the fluorescence intensity emitted by the samples tested at the wavelength of 485 nm, as well as the standard deviation and the percentage error about the five tests performed for each element.

4.2. Calibration test of the experimental sensor

The laboratory tests using the proposed sensor were performed by inserting it inside a tube that exactly reproduces the sensor-holder of the buoy. This tube was, from time to time, inserted into five beakers. The first containing clean seawater, the others containing seawater with a surface layer of one of the hydrocarbons tested with the spectrophotometer and taken from the same samples.

The percentage of 3.47 % of pollutant was added to each beaker, obtaining a surface layer s = 1 mm thick, for the reasons already specified in the previous section. After a waiting time of 10 minutes, to allow the liquid charged by the pump to stabilize in the chamber, to eliminate the air bubbles and to thicken the pollutant on the surface, each of the five measurements planned for each of the four samples analysed, was performed.

After a thoughtful choice of sensor components and control electronics, no significant differences were obtained in the response of the sensor when the distance of the LED/detector system from the water surface inside the sensor-measuring chamber varied (adjustment carried out with the bracket/ threaded screw system). This is because this distance is very short (< 10 mm). It can therefore be said that the device is optimized to excite and, consequently, measure the maximum intensity of emerging radiation.

The average of the sensor responses (band-pass filter at 485 nm), for excitation wavelength λ_{ex} = 235 nm, is shown in Figure 10, the sensor output is in mA (*Gain* = 1000). To compare the data detected by the sensor with those obtained using the spectrofluorometer, the normalized fluorescence unit (lx) is shown on the secondary axis. This figure also shows the standard deviation of the five measurements made for each sample. The results of the different tests are summarized in Table 3.

Finally, in order to evaluate the response of the sensor as a function of the thickness of a polluting patch on the surface of seawater, further tests were carried out using the same compounds. For this purpose, the quantity of the single polluting compound was increased, from time to time, compared to the

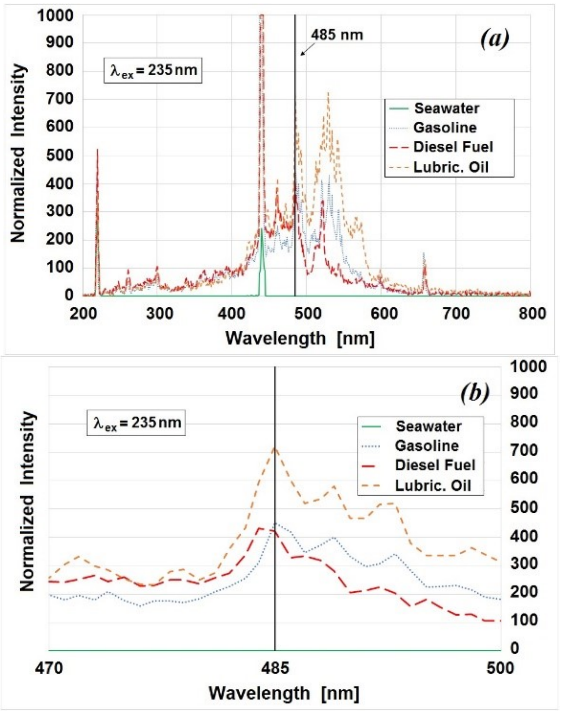

Figure 9. (*a*) Spectrofluorometric spectra of samples. (*b*) Detail of the spectrum around 485 nm.

volume of seawater contained in the beaker, until reaching a surface thickness of 1 mm. The detection of the emitted fluorescence was performed in steps, according to the scheme described in Table 4. The values obtained represent the average for three samples relating to each measured thickness. The percentage error calculated on each series remained around 4 %.

Figure 11 shows the trend of the sensor response as a function of the surface thickness of the pollutant.

5. RESULTS AND DISCUSSION

The last row of Table 3 shows the ratios between the averages of the spectrofluorimeter responses (Table 2) and those of the sensor responses for the respective tested elements, at the wavelength λ_{em} = 485 nm, for an excitation wavelength λ_{ex} = 235 nm. The fact that the ratios relating to the tested hydrocarbons remain rather constant around the value 4, despite measuring non-pure compounds and therefore subject to local variations in fluorescence, indicates that the sensitivity of the sensor is approximately ¼ lower than that of the spectrofluorometer.

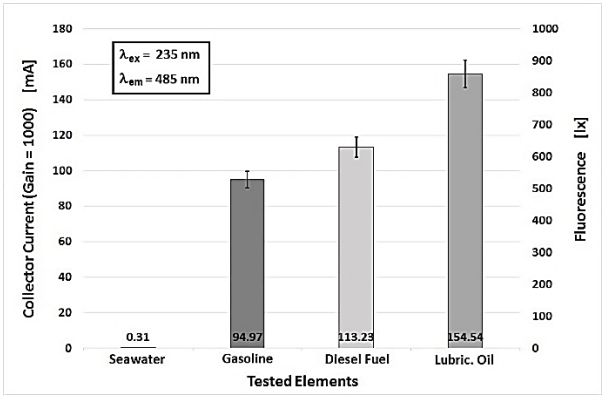

Figure 10. Response of the sensor on 485 nm.

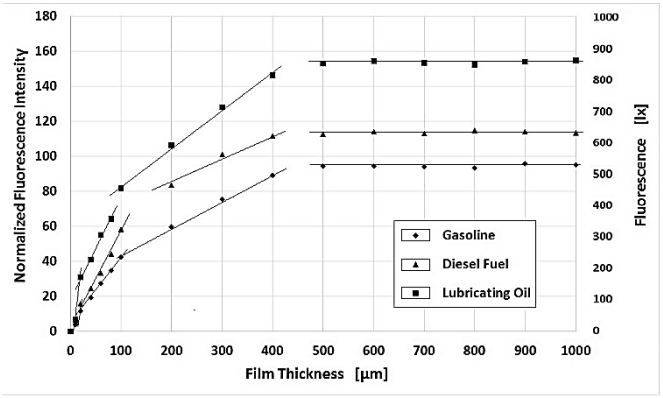

Figure 11. Response of the sensor as a function of the thickness of a pollutant slick on the surface of seawater.

It can be asserted that the tendency of the sensor to provide values proportional to those detected by the laboratory spectrofluorimeter makes the sensor able to distinguish the characteristic fingerprint of each element tested. Of course, these are compounds, not individual aromatic hydrocarbons. The latter would provide even more distinguishable relationships.

The graphs of the fluorescence intensity values of the various samples of the tested elements, summarized in Table 3, are shown in Figure 12. Furthermore, the linear best-fits of the five measured values for each tested item were plotted.

Although the repeatability test of the measurement process should be performed by keeping all the measurement conditions unchanged and evaluating how repeatable the results are, in the present case, while maintaining the same operator and the same measurement device, tests were carried out on five samples different for each type of hydrocarbon. Therefore, it could be argued that the comparison between the measurements carried out, only provides an estimate of the repeatability of the UV sensor. Although these are not orthodox conditions, the authors believe it is acceptable to obtain information on the repeatability of the results by evaluating their deviation from the linear best-fit calculated on the five measurements performed. It is

Table 2. Fluorescence intensity of tested elements for λ_{ex} = 235 nm and λ_{em} = 485 nm.

	Seawater	Gasoline	Diesel Fuel	Lubric. Oil
Average	0.70	451	433	751
St. Dev.	0.04	18	18	31
% Error	5.2	4.1	4.2	4.1

Table 3. Summary of results for different tests on hydrocarbons. The results are given in mA.

	Seawater	Gasoline	Diesel Fuel	Lubr. Oil
Test #1	0.3	91.3	119.2	159.2
Test #2	0.3	100.7	108.3	153.7
Test #3	0.3	96.2	107.3	149.1
Test #4	0.3	91.7	113.2	147.2
Test #5	0.3	94.9	118.0	163.5
Average	**0.30**	**95**	**113**	**155**
St. Dev.	**0.02**	**4**	**5**	**7**
% Error	5.1	4.0	4. 8	4.4
Ratios	2.1	4.7	3.9	4.7

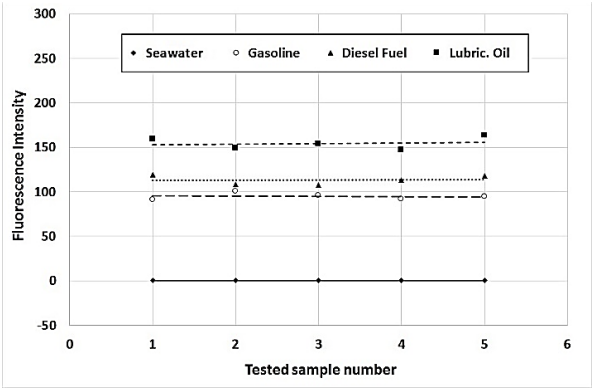

Figure 12. Trend of fluorescence intensity values of the different tested elements, expressed in mA.

concluded that the deviation from linearity, contained within 3% for the four elements tested, can indicate a good repeatability of the results obtained.

As regards the detection of fluorescence as the surface thickness of the pollutant changes, from the graph in Figure 11 we can see that the first significant responses for all tested compounds were obtained around 10 µm-thickness, which can be considered as the lower reading limit for the sensor (resolution). Subsequently, a linear dependence of the sensor sensitivity as the thickness varied up to approximately 100 µm was noted. In the range of 200 µm - 400 µm, the response remained linear but with a lower slope, while beyond 500 µm up to a thickness of 1000 µm, the signal remained constant for all the samples tested. The results obtained fit well with the data present in the most recent scientific literature [46]-[48].

Table 5 summarizes both the linear regression equation and the determination coefficient of the different ranges that compose the trend of the sensor response as the surface thickness of the pollutant changes.

Table 4. Example of a test measuring fluorescence as the thickness of the surface hydrocarbon layer varies.

Thickness in µm	Volume* in ml	Gasoline Average±SD in mA	Diesel Fuel Average±SD in mA	Lubric. Oil Average±SD in mA
0	0	0.29 ± 0.01	0.30 ± 0.01	0.30 ± 0.01
2	0.034	0.33 ± 0.01	0.37 ± 0.01	0.41 ± 0.01
4	0.068	0.35 ± 0.01	0.36 ± 0.01	0.42 ± 0.01
6	0.102	0.38 ± 0.01	0.40 ± 0.01	0.47 ± 0.02
8	0.136	0.53 ± 0.02	0.62 ± 0.02	0.74 ± 0.02
10	0.17	3.65 ± 0.05	5.36 ± 0.07	6.70 ± 0.07
20	0.34	11.4 ± 0.3	15.6 ± 0.2	30.7 ± 0.4
40	0.68	19.4 ± 0.3	24.4 ± 0.3	41.0 ± 0.6
60	1.02	27.4 ± 0.4	33.2 ± 0.4	55.0 ± 0.8
80	1.36	34.7 ± 0.5	44.3 ± 0.6	64.1 ± 0.8
100	1.70	42.4 ± 0.6	58.4 ± 0.8	81.8 ± 1.0
200	3.40	59.7 ± 0.8	83.4 ± 1.1	106.4 ± 1.5
300	5.10	75.3 ± 1.1	100.9 ± 1.4	128.2 ± 1.5
400	6.80	89.0 ± 1.2	111.4 ± 1.5	146.3 ± 1.9
500	8.50	94.3 ± 1.3	112.6 ± 1.5	152.9 ± 2.0
600	10.20	94.2 ± 1.3	114.0 ± 1.6	154.4 ± 2.0
700	11.90	93.9 ± 1.2	113.0 ± 1.5	153.4 ± 2.0
800	13.60	93.3 ± 1.2	114.7 ± 1.6	152.4 ± 2.0
900	15.30	95.7 ± 1.3	114.0 ± 1.6	153.9 ± 2.0
1000	17.00	95.0 ± 1.3	113.2 ± 1.5	154.5 ± 2.0

* Volume of pollutant for a 500 ml-volume of seawater.

Table 5. Linear Regression equation and Determination Coefficient of different ranges of the sensor response trend as a function of the variation in the surface thickness of the pollutant.

Pollutant	Surface Thickness Ranges in µm		
	20 - 100	200 - 400	500 - 1000
Gasoline	Y = 0.39 X + 3.87	Y = 0.15 X + 30.72	Y = 0.0021 X + 92.81
	R^2 = 0.9898	R^2 = 0.9984	R^2 = 0.9994
Diesel Fuel	Y = 0.53 X + 3.53	Y = 0.14 X + 56.57	Y = 0.0013 X + 112.60
	R^2 = 0.9926	R^2 = 0.9793	R^2 = 0.9999
Lubric. Oil	Y = 0.63 X + 16.93	Y = 0.20 X + 67.12	Y = 0.0016 X + 152.40
	R^2 = 0.9898	R^2 = 0.9926	R^2 = 0.9998

From the graph in Figure 11, two important considerations can be drawn:

1. the sensor is able to identify very thin hydrocarbon slicks (≥ 10 µm);
2. above 500 µm of thickness, the pollutant emits the entire fluorescence excitable by UV light.

6. CONCLUSION

An inexpensive and low electrical consumption sensor was designed to locate, on board a sensor-buoy, the presence of aromatic hydrocarbons on the surface of coastal marine waters of the Mediterranean Sea. This goal was achieved by detecting the UV-induced fluorescence produced by aromatic hydrocarbons.

A deep UV-LED emitting a 235 nm - wavelength was used as a light source to replace the UV laser, guaranteeing satisfactory performances despite the low cost. The spectrofluorometric system, consisting of a phototransistor shielded by a 485 nm - bandpass filter, made it possible to capture and enhance exclusively the fluorescence signal relating to hydrocarbons, eliminating the disturbance produced by the fluorescence of chlorophyll-*a* or CDOM possibly present on the surface of the seawater.

The experimental tests carried out on the most common hydrocarbons in the sea have shown that the sensor object of this study has good repeatability (linearity less than 3 %), accuracy (percentage error around 4 %), and sensitivity (about ¼ compared to that of a laboratory spectrofluorometer).

The sensor was also tested by varying the thickness of the pollutant slick, showing the ability to measure a monolayer 10 µm thick. Finally, in addition to the low cost and the low power supply requirement (less than 6 V), the sensor is flexible, being able to accommodate LEDs of different wavelengths or LED arrays to match the fluorescence characteristics of the tested items.

REFERENCES

[1] W. Hongyi, X. Ling, W. Yuchen., C. Liwei, J. Bian, C. Xiaohai, W. Yinglin, Improving cleaner production of human activities to mitigate total petroleum hydrocarbons accumulation in coastal environment. Mar. Pollut. Bull. 186 (2023) 114473. DOI: 10.1016/j.marpolbul.2022.114473

[2] F. Cyr, M. Tedetti, F. Besson, N. Bhairy, M. Goutx, A Glider-Compatible Optical Sensor for the Detection of Polycyclic Aromatic Hydrocarbons in the Marine Environment. Frontiers in Marine Science 6 (2019) 110. DOI: 10.3389/fmars.2019.00110

[3] Z Asif, Z. Chen, C. An, J. Dong, Environmental impacts and challenges associated with oil spills on shorelines. J. Mar. Sci. Eng. 10 (2022) 6, pp. 762-781.
DOI: 10.3390/jmse10060762

[4] J. Z. Wang, Y. F. Guan, H. G. Ni, X. L. Luo, E. Y. Zeng, Polycyclic aromatic hydrocarbons in riverine runoff of the Pearl River Delta (China): concentrations. fluxes. and fate. Environ. Sc. And Technol. 41 (2007) 16, pp. 5614-5619.
DOI: 10.1021/es070964r

[5] M. Tsapakis, E. G. Stephanou, I. Karakassis, Evaluation of atmospheric transport as a nonpoint source of polycyclic aromatic hydrocarbons in marine sediments of the Eastern Mediterranean. Mar. Chem. 80 (2003) 4, pp. 283-298.
DOI: 10.1016/S0304-4203(02)00132-9

[6] A. S. Neroda, A. A. Goncharova, V. F. Mishukov, PAHs in the atmospheric aerosols and seawater in the North-West Pacific ocean and Sea of Japan. Atmos. Environ. 222 (2019), pp. 117117
DOI: 10.1016/j.atmosenv.2019.117117

[7] T. M. Alves, E. Kokinou, G. Zodiatis, R. Lardner, C. Panagiotakis, H. Radhakrishnan, Modelling of oil spills in confined maritime basins: the case for early response in the Eastern Mediterranean Sea. Environ. Pollut. 206 (2015) pp. 390-399.
DOI: 10.1016/j.envpol.2015.07.042

[8] EEA (European Environmental Agency), State of Europe's seas, EEA report No. 2/2015, 2015. Online [Accessed 19 November 2024]
https://www.eea.europa.eu/publications/state-of-europes-seas

[9] C. Rizzi, S. Villa, C. Chimera, A. Finizio, G. S. Monti, Spatial and temporal trends in the ecological risk posed by polycyclic aromatic hydrocarbons in Mediterranean Sea sediments using large-scale monitoring data. Ecol. Indic. 129 (2021), pp. 107923-107935.
DOI: 10.1016/j.ecolind.2021.107923

[10] A. Saliot, C. Andrie, R. Hô, J. C. Marty, Occurrence and fate in the sediment and in the water column. as dissolved and associated with small and large size particulates. Int. J. Environ. Anal. Chem. 22 (1985), pp. 25-46.
DOI: 10.1080/03067318508076407

[11] Y. Hou, Y. Li, G. Li, X. Tong, Y. Wang, Oil-spill detection sensor using ultraviolet-induced fluorescence for routine surveillance in coastal environments. Appl. Phys. B: Lasers Opt. 128 (2022) 41, pp. 41-49.
DOI: 10.1007/s00340-021-07741-3

[12] A. Louvado, N. Gomes, M. M. Q. Simões, A. Almeida, D. F. R. Cleary. A. Cunha, Polycyclic aromatic hydrocarbons in deep sea sediments: microbe-pollutant interactions in a remote environment. Sci. Total Environ. 526 (2015), pp. 312-328.
DOI: 10.1016/j.scitotenv.2015.04.048

[13] World Health Organization, Overall Evaluations of Carcinogenicity: An Updating of IARC Monographs, 1-42, 10-18 March 1987, ISBN 92-832-1411-0. Online [Accessed 19 November 2024]
https://www.ncbi.nlm.nih.gov/books/NBK533509/

[14] S. Felemban, P. Vazquez, E. Moore, Future Trends for In Situ Monitoring of Polycyclic Aromatic Hydrocarbons in Water Sources: The Role of Immunosensing Techniques. Biosensors 9 (2019) 4, pp. 142-157.
DOI: 10.3390/bios9040142

[15] Q. Xinga, L. Lia, M. Loua, L. Binga, R. Zhaoc, Z. Li, Observation of oil spills through Landsat thermal infrared imagery: a case of deepwater horizon. Aquatic Procedia. 3 (2015), pp. 151-156.
DOI: 10.1016/j.aqpro.2015.02.205

[16] Y. Chen, Z. Wang, Marine Oil spill detection from SAR images based on attention U-Net model using polarimetric and wind speed information. Int. J. Environ. Res. Public Health. 19 (2022), pp. 12315-12325.
DOI: 10.3390/ijerph191912315

[17] Science Education through Earth Observation for High Schools (SEOS), Remote Sensing Using Lasers, Online [Accessed 19 November 2024]
https://seos-project.eu/laser-rs/laser-rs-c01-p04.html

[18] J.H. Moon, M. Jung, Geometrical Properties of Spilled Oil on Seawater Detected Using a LiDAR Sensor, Journal of Sensors 2020 (2020) 5609168.
DOI: 10.1155/2020/5609168

[19] S. A. Khan, M. Z. Alam, M. Mohasin, S. Ahmad, U. Salma, H. Parveen, S. Mukhtar, M. Al-Anazi, (+ 2 more authors), Ultrasound-Assisted Synthesis of Chalcone: A Highly Sensitive and Selective Fluorescent Chemosensor for the Detection of Fe3+ in Aqueous Media, J. Fluoresc 34 (2023), pp. 723-728.
DOI: 10.1007/s10895-023-03317-w

[20] S. A. Nsibande, H. Montaseri, P. B. C. Forbes, Advances in the application of nanomaterial-based sensors for detection of polycyclic aromatic hydrocarbons in aquatic systems. Trends Anal. Chem. 115 (2019), pp. 52-69.
DOI: 10.1016/j.trac.2019.03.029

[21] C. M. Reddy, J. G. Quinn, GC-MS analysis of total petroleum hydrocarbons and polycyclic aromatic hydrocarbons in seawater samples after the North Cape oil spill. Mar. Pollut. Bull. 38 (1999), pp. 126-135.
DOI: 10.1016/S0025-326X(98)00106-4

[22] M. H. Habibi, M. R. Hadjmohammadi, Determination of Some Polycyclic Aromatic Hydrocarbons in the Caspian Seawater by HPLC Following Preconcentration with Solid-Phase Extraction. Iran J. Chem. Chem. Eng. 27 (2008), pp. 91-96.
DOI: 10.30492/ijcce.2008.6951

[23] J. N. Huckins, M. W. Tubergen, G. K. Manuweera, Semipermeable membrane devices containing model lipid: A new approach to monitoring the bioavaiiability of lipophilic contaminants and estimating their bioconcentration potential. Chemosphere 20 (1990) 5, pp. 533-552.
DOI: 10.1016/0045-6535(90)90110-F

[24] X. X. Han, R. S. Rodriguez, C. L. Haynes, Y. Ozaki, B. Zhao, Surface-enhanced Raman spectroscopy. Nat Rev Methods Primers. 87 (2021).
DOI: 10.1038/s43586-021-00083-6

[25] X. Shi, D. Zhang, W. Jia, X. Yan, J. Yang, C. Wang, J. Ma, Portable Surface-Enhanced Raman Scattering Sensor for the Rapid Detection of Polycyclic Aromatic Hydrocarbons in Coastal Seawater. Marine Technology Society Journal 53 (2019) 2, pp. 46-55.
DOI: 10.4031/MTSJ.53.2.5

[26] P. Rohde, J. A. Busch, R. H Henkel, D. Voss, O. Zielinski, Detection and identification of hydrocarbons in marine waters using time resolved laser-fluorescence: Set-up and first results of a new submersible sensor, Proc. of Oceans 2009-Europe, Bremen, Germany, 11-14 May 2009.
DOI: 10.1109/OCEANSE.2009.5278101

[27] B. Gong, H. Zhang, X. Wang, K. Lian, X. Li, B. Chen, H. Wang, X. Ni, Ultraviolet-induced fluorescence of oil spill recognition using a semi-supervised algorithm based on thickness and mixing proportion–emission matrices. Anal. Methods 13 (2023), pp. 1649-1660.
DOI: 10.1039/D2AY01776H

[28] Y. Li, S. Yoshida, Y. Chondo, H. Nassar, N. Tang, Y. Araki, A. Toriba, T. Kameda, (+1 more author). On-Line Concentration and Fluorescence Determination HPLC for Polycyclic Aromatic Hydrocarbons in Seawater Samples and Its Application to Japan Sea, Chem. Pharm. Bull. 60 (2012) 4, pp. 531–535.
DOI: 10.1248/cpb.60.531

[29] A. Marrucci, B. Marras, S. S. Campisi, M. Schintu, Using SPMDs to monitor the seawater concentrations of PAHs and PCBs in marine protected areas (Western Mediterranean). Mar. Pollut. Bull. 75 (2013) 1-2, pp. 69-75.
DOI: 10.1016/j.marpolbul.2013.08.004

[30] D. Patra, Applications and New Developments in Fluorescence Spectroscopic Techniques for the Analysis of Polycyclic Aromatic Hydrocarbons. Appl. Spectrosc. Rev. 38 (2003), pp. 155-185.
DOI: 10.1081/ASR-120021166

[31] S. M. Rudnick, R. F. Chen, Laser-induced fluorescence of pyrene and other polycyclic aromatic hydrocarbons (PAH) in seawater, Talanta 47 (1998) 4, pp. 907-919.
DOI: 10.1016/S0039-9140(98)00160-X

[32] Y. Hou, Y. Li, Y. Liu, G. Li, Z. Zhang, Effects of polycyclic aromatic hydrocarbons on the UV-induced fluorescence spectra of crude oil films on the sea surface. Mar. Pollut. Bull. 146 (2019) pp. 977-984.
DOI: 10.1016/j.marpolbul.2019.07.058

[33] D. Alizzio, M. Bonfanti, N. Donato, C. Faraci, G. M. Grasso, F. Lo Savio, R. Montanini, A. Quattrocchi, Design and performance evaluation of a "fixed-point" spar buoy equipped with a piezoelectric energy harvesting unit for floating near-shore applications. Sensors. 21 (2021) 5, pp. 1912-1929.
DOI: 10.3390/s21051912

[34] S. J. Hart, R. D. JiJi, Light emitting diode excitation emission matrix fluorescence spectroscopy. Analyst 127 (2002) 12, pp. 1693-1699.
DOI: 10.1039/B207660H

[35] Y. Li, P. N. Nesterenko, B. Paull, R. Stanley, M. Macka, Performance of a New 235 nm UV-LED-Based On-Capillary Photometric Detector. Anal. Chem. 88 (2016) 24, pp. 12116-12121.
DOI: 10.1021/acs.analchem.6b02832

[36] A. Sharma, S. G. Schulman, Introduction to Fluorescence Spectroscopy, Wiley-Interscience, June 1999, ISBN: 978-0-471-11098-9.

[37] D. Seo, S. Oh, S. Shin, M. Lee, Y. Hwang, S. Seo, Smartphone compatible on-site fluorescence analyzer for spilled crude oil based on CMOS image sensor. Sens. Actuator B Chem. 289 (2019), pp. 93-99.
DOI: 10.1016/j.snb.2019.03.086

[38] P. Karlitschek, F. Lewitzka, U. Bünting, M. Niederkrüger, G. Marowsky, Detection of aromatic pollutants in the environment by using UV-laser-induced fluorescence. Appl. Phys. B Lasers Opt. 67 (1998), pp. 497-504.
DOI: 10.1007/s003400050535

[39] S. Landgraf, Use of ultrabright LEDs for the determination of static and time-resolved fluorescence information of liquid and solid crude oil samples. J. Biochem. Bioph. Meth. 61 (2004), pp. 125-134.
DOI: 10.1016/j.jbbm.2004.04.003

[40] A. V. Sharikova, D. K. Killimger, Laser- and UV-LED-Induced Fluorescence Detection of Drinking Water and Water-Dissolved Organics, Laser Applications to Chemical. Security and Environmental Analysis 17–20 March 2008 St. Petersburg. Florida United States.
DOI: 10.1364/BIOMED.2008.JMA34

[41] J. P. Harringmeyer, K. Kaiser, D. R. Thompson, M. Gierach, C. L. Cash, C. G. Fichot, Detection and sourcing of CDOM in urban coastal waters with UV-visible imaging spectroscopy. Front. Environ. Sci. 9 (2021), art. no. 647966.
DOI: 10.3389/fenvs.2021.647966

[42] X. G. Xing, D. Z. Zhao, Y. G. Liu, J. H. Yang, P. Xiu, L. Wang, An Overview of Remote Sensing of Chlorophyll Fluorescence. Ocean Sci. 42 (2007), pp. 49-59.
DOI: 10.1007/BF03020910

[43] M. V. Bills, A. Loh, K. Sosnowski, B. T. Nguyen, S. Yong Ha, U. H. Yim, J. Y. Yoon, Handheld UV fluorescence spectrophotometer device for the classification and analysis of petroleum oil samples. Biosens. Bioelectron. 159 (2020), pp. 112193.
DOI: 10.1016/j.bios.2020.112193

[44] D. V. Manov, G. C. Chang, T. D. Dickey, Methods for Reducing Biofouling of Moored Optical Sensors. J. Atmos. Ocean. Technol. 21 (2003), pp. 958-968.
DOI: 10.1175/1520-0426(2004)021<0958:MFRBOM>2.0.CO;2

[45] F. P. Chavez, D. Wright, R. Herlien, M. Kelley, F. Shane, P. G. Strutton, A Device for Protecting Moored Spectroradiometers from Biofouling. J. Atmos. Ocean. Technol. 17 (2000), pp. 215-219.
DOI: 10.1175/1520-0426(2000)017<0215:ADFPMS>2.0.CO;2

[46] A. B. Utkin, A. Lavrov, R. Vilar, Evaluation of oil spills by laser induced fluorescence spectra, Proceedings V. 7994. LAT 2010: International Conference on Lasers, Applications, and Technologies, 77994, 7 February 2011.
DOI: 10.1117/12.880750

[47] W. Jiang, J. Li, X. Yao, E. Forsberg, S. He, Fluorescence Hyperspectral Imaging of Oil Samples and Its Quantitative Applications in Component Analysis and Thickness Estimation, Sensors 18 (2018), pp. 4415-4424.
DOI: 10.3390/s18124415

[48] O. Bukin, D. Proschenko, C. Alexey, D. Korovetskiy, I. Bukin, V. Yurchik, I. Sokolova, A. Nadezhkin, New Solutions of laser-induced fluorescence for oil pollution monitoring at sea. Photonics 7 (2020) 2, pp. 36-51.
DOI: 10.3390/photonics7020036.